Numerical Modeling for Novel Solar Air Heater Utilizing Wax Paraffin-PCM

Salah M. Salih
Power-Mechanical Engineering Department
Al-Furat Al-Awsat Technical University
Engineering Technical College of Al-Najaf
salahmahditech @yahoo.com

Saleh E. Najim
Mechanical Engineering Department
University of Basra
Engineering College
pro.salehin52 @yahoo.com

Jalal M. Jalil
Electro-mechanical Engineering Department
University of Technology
Engineering College
jalalmjalil @gmail.com

Abstract— **A mathematical model to analysis three–dimensional forced convection turbulent flow in a novel solar air heater integrated with multiple rectangular capsules filled by paraffin wax-based on phase change material PCM was implemented. The investigations were performed under three airflow speed of (0.6, 1.2, and 1.8) kg/min and average solar flux of 625 W/m^2. The results revealed that the delaying melting time and also lower the melting temperature of PCM by increasing airflow speed during the charging process. As well as, the freezing period is dependent on the airflow speed by inverse relation. Also, the data results represent that the useful energy rate and thermal storage efficiency were a strong dependence on the airflow speed. Moreover, it can be detected that the optimal freezing time and the air temperature rise of the heater were reached about 210 minutes with (12 – 1.5 °C), 150 minutes with (7.5 – 1.4°C), and 120 minutes with (5.5 – 1.5 °C), at airflow speed of 0.6, 1.2, and 1.8 kg/min, respectively, which can be used at night to supply some applications by thermal energy such as heating buildings and drying agricultural crops.**

Keywords*—*Double-Pass Solar Heater, Phase Change Material PCM, Thermal Conductivity Enhancement,

1. INTRODUCTION

Sunshine energy is the most abundant natural resource for humankind and a promising source of clean energy for wide-ranging usage. In the 21st century, recent researches indicate that climate change in the Earth due to the problems of global warming. Due to the high emissions levels resulting from the consumption of more than 81% of fossil fuels like oil, coal, and gas to produce conventional energy in the world[1]. Besides more toxic gases such as carbon dioxide CO_2 and nitrous oxide N_2O which are unprecedented in past decades, which cause a lot of serious lung diseases that threaten the life of mankind if it has not been seriously tackled this problem.

Through these challenges, it is incumbent on all countries including Iraq, to look for alternative sources of energy more effectively, especially as it suffers from a severe shortage in the provision of electricity. Solar air heaters are considered a significant technology of the solar thermal usages that contributes to the conservation of fossil energy and eco-friendly way. Accordingly, it can be guided economically and practically in thermal engineering applications through flat-plate solar air heater SAH. To convert collected energy into a hot air at low-temperature applications such as space heating of buildings and glasshouse, or solar drying of agricultural and industrial purposes operated ineffectively without some form of thermal energy storage, as reviewed comprehensively by authors [2-5]. The Sun emits millions of watts of energy rate that intercepted by the Earth through solar radiation every day and lies approximately of 150 million km from the Sun. Nearly 51% of the total incoming solar radiation arrives the Earth surface, and the rest 49% is returned into space and received by the environment [6].In addition, the incompatibility between access to sunlight during the day and the need to request heat energy after sunset. Therefore, it needs many theoretical and practical studies to achieve the optimal performance of thermal energy needs at all times for different applications in terms of design and productivity.

Thermal storing energy integrated with the solar heater can play an essential role to overcome this problem. Modern research of the solar thermal storage units focused on latent storing energy-based on a solid/liquid phase change material PCM like a paraffin wax has the highest capacity for storing energy. PCMs have the ability to absorb and release a large amount of energy at an almost constant temperature during melting/freezing processes. Although the phase change material PCM is a safe and obtainable form, it is a low-thermal conductive is a significant drawback. Numerous studies have provided a range of technique resolves to increase PCM conductivity such as; nanoparticles or encapsulation technology of the PCM [7, 8], and usage of the longitudinal fins or porous materials in the PCM [9, 10].

Fath[8] researched the conventional-SAC performance integrated with encapsulated PCM with a melting temperature of 50 °C. A corrugated set of an encapsulated copper cylindrical was packed with paraffin wax as PCM and located as absorbent and container of the energy store. The system was taken a 1.0 m^2 of a collected area, and 7.5 cm of the height of the collector channel. The investigation showed that the daily efficiency of the staggered set tube with PCM is approximate of 63.35% which was under an air MFR of 0.02 kg/s. It was also detected that the exit temperature of air increased by 5 $^{\circ}$C from ambient temperature and extended for about 16 hr, whereas the daily efficiency of flat plate-SAC has 38.7% for 9 hr. Charvat et al.[11] carried out an experimental and numerical study to evaluate the effect of PCM on a solar air collector SAC performance. The MATLAB code used for modeling SAC was integrated with paraffin wax as PCM has a melting temperature of 40 ◦C. They observed that the lower

exit air temperatures with energy storing during the charging period, and higher air temperatures at the discharging period process. From the previous literature, there is a specified gap in the analysis of a double-pass solar heater performance applying PCM as latent storing energy. Karim and Hawlader [12] studied experimentally and theoretically the performance of three different types of SAHs. It was found that the corrugated solar heater efficiency was of 10–15% more than the conventional heater. Besides, results revealed that the performance of a dual-pass SAH was better than all three types of the heater. Mathematical analysis of the thermal performance of the single and double-pass SAH without and with porous material was performed by Yousef and Adam [13]. They showed that the performance of the dual-pass SAH was better by 10-12% than the single pass-SAH, at the same operating conditions. It was also observed that the increment in the energy efficiency by 8% of the collector by using a porous medium as compared to another collector non-porous.

This paper purposes to analysis a novel design of the double-pass solar air heater DP-SAH performance integrated with paraffin wax-PCM by using encapsulation technology to improve thermal conductivity of PCM. Furthermore, the influence of the airflow speed on the temperature distribution of airflow and paraffin wax inside storage container, thermal storage efficiency, and melting/freezing time of paraffin wax-PCM was studied numerically.

2. Computational Modeling

In this study, under an ambient temperature of 25 $^{\circ}$C, wind speed of 1.5 m/s, airflow speed range of (0.6, 1.2, and 1.8) kg/min, and solar flux about 625 W/m^2 to study thermal performance of a double-pass solar heater that includes of two passages. Firstly, air flows in the lower duct (1st pass flow) which is formed between the lower absorber surface and back plate of the heater. Secondly, recycle air flows through the upper duct (2nd pass flow) which is formed between the glass cover and the upper absorber surface and container of PCM. The test section consists of (1200×320mm), and air gap of (84mm) which was left at the end for air flowing towards the upper channel. In addition, the aspect ratio (W/H) is kept as 10 for the upper and lower passage of the heater which is (32mm) gap height respectively, according to ASHRAE standards, [14].

Figure (1) shows the problem geometry consists of the following elements: 3 mm thick of the transparent cover, 32 mm of the air gap for each channel of a two-pass solar heater, multiple rectangular PCM encapsulation as absorbent and storage unit (1 mm thick of the galvanized iron GI-absorbent plate, and a 18 mm thick paraffin wax layer), 1 mm thick of the GI-back plate of the solar heater. The length and width of the heater are 1284 mm and 320 mm, respectively. Table 1 involves physical coordinates of the current problem.

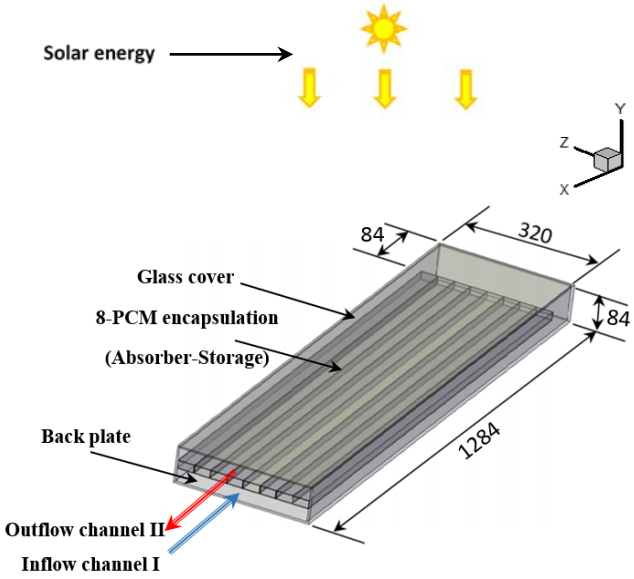

Fig. 1. Physical coordinates of problem.

Table 1 Specifications of problem.

Parameter	Values
DP-SA heater:	
Length	1284 mm
Width	320 mm
Height	84 mm
Channel height	32 mm
Effective glazing area	0.411 m^2
Glass thickness	3 mm
Glass transmittance	0.83
Galvanized iron absorbance	0.9
Galvanized iron thickness	1 mm
PCM rectangular capsules:	
Number of capsules	8
Length	1200 mm
Width	40 mm
Height	20 mm
Thickness	1 mm
Total weight of paraffin wax PCM	5 kg

In this current study, the new contribution used eight rectangle pipes of galvanized iron (GI) filled with RT42 paraffin wax-PCM due to the low conductivity for paraffin wax in the three transition phases, were installed as multiple capsules of latent storing energy in the middle of the DP-SAH height. Each capsule of storage contains 0.625 kg of paraffin wax- PCM which was placed parallel to the airflow and coated with black matte as an absorbent material. These storage multiple-capsules worked as an absorbent for solar irradiation so that the storing thermal energy. Table 2 presents the thermal properties of paraffin wax-PCM which used as a storage material[15].

Table 2 Thermo-physical properties of paraffin wax- PCM, [15].

Property	Values
Solidus temperature, T_{m1}	38°C
Liquidus temperature, T_{m2}	43°C
Heat storage capacity	174 kJ/kg
Specific heats in both solid and liquid states	2 kJ. kg^{-1}.K^{-1}
Density in solid state	880 kg.m^{-3}
Density in liquid state	760 kg.m^{-3}
Volume expansion (solid/liquid phase change)	16%
Thermal conductivity in both solid and liquid states	0.2 W.m^{-1}. K^{-1}

To analyze and construct the mathematical model of the governing equations of the two-pass solar air heater integrated with paraffin wax-PCM as latent storing energy can be simplified under the following assumptions:

i. Incompressible, three-dimensional and turbulent flow.
ii. The DP-SAH is in a quasi-steady state, and air properties are assumed an independent of temperature.
iii.
iv. Paraffin wax-PCM is isotropic, and its phase transition occurs at a temperature range from 38 to 43 °C. PCM is a transient conduction of energy storage.
v. Thermal inertias are negligible, and no-leakage airflow in the test section.
vi. As the width of the DP-SAH is much smaller than its length, very little temperature difference happens. Consequently, analyses are based on the symmetrical model in the z-direction.

In this mathematical model, the staggered grid of finite volume SIMPLE algorithm [16] has been formulated in a FORTRAN language. To analyze a thermal-fluid flow of three-dimensional forced convection within the first and second channel of a two-pass solar heater under the above assumptions. The continuity, momentum, energy in addition to the turbulence model (k-ε)proposed by Launder and Spalding[17] can be written in a general form as:

$$\frac{\partial}{\partial x}(\rho U\phi)+\frac{\partial}{\partial y}(\rho V\phi)+\frac{\partial}{\partial z}(\rho W\phi)=\frac{\partial}{\partial x}\left(\Gamma_\phi\frac{\partial\phi}{\partial x}\right)+\frac{\partial}{\partial y}\left(\Gamma_\phi\frac{\partial\phi}{\partial y}\right)+\frac{\partial}{\partial z}\left(\Gamma_\phi\frac{\partial\phi}{\partial z}\right)+S_\phi \quad \dots(1)$$

In this equation, the convection terms expressions are on the left while the diffusion and source expressions are on the right. Table 3 represents the source expression appearing in Eq. (1).

Table 3. Source term in the governing (PDES).

Equation	ϕ	Γ_ϕ	S_ϕ
Continuity	1	0	0
U-momentum	U	Γ_u	$-\frac{\partial P}{\partial x}+\frac{\partial}{\partial x}\left(\nu_e\frac{\partial U}{\partial x}\right)+\frac{\partial}{\partial y}\left(\nu_e\frac{\partial V}{\partial x}\right)+\frac{\partial}{\partial z}\left(\nu_e\frac{\partial W}{\partial x}\right)$
V-momentum	V	Γ_v	$-\frac{\partial P}{\partial y}+\frac{\partial}{\partial x}\left(\nu_e\frac{\partial U}{\partial y}\right)+\frac{\partial}{\partial y}\left(\nu_e\frac{\partial V}{\partial y}\right)+\frac{\partial}{\partial z}\left(\nu_e\frac{\partial W}{\partial y}\right)$
W-momentum	W	Γ_w	$-\frac{\partial P}{\partial z}+\frac{\partial}{\partial x}\left(\nu_e\frac{\partial U}{\partial z}\right)+\frac{\partial}{\partial y}\left(\nu_e\frac{\partial V}{\partial z}\right)+\frac{\partial}{\partial z}\left(\nu_e\frac{\partial W}{\partial z}\right)$
Temperature	T	Γ_e	0
Kinetic energy	K	Γ_k	G-ε
Dissipation rate	ε	Γ_ε	$C_{1\varepsilon}\frac{\varepsilon}{k}G-C_{2\varepsilon}\frac{\varepsilon^2}{k}$

Where $\Gamma_k=\frac{\upsilon_t}{\sigma_k}$, $\Gamma_\varepsilon=\frac{\upsilon_t}{\sigma_\varepsilon}$, $\Gamma_u=\Gamma_v=\Gamma_w=\upsilon_e$,

The empirical constants for (k − ε) model

$C_\mu=0.09$, $C_{1\varepsilon}=1.44$, $C_{2\varepsilon}=1.92$, $\sigma_k=1.00$, $\sigma_\varepsilon=1.30$

In general, the temperature distribution of the solid surfaces such as; the glazed cover, the upper and lower absorbent surfaces, and back plate of the solid two-pass solar heater components, which represented in the same approach from the balancing equations of energy were achieved in three sub-models coupled within the main program in order to solve the governing energy equations of the system simultaneously.

The air flowing in both 1st and 2nd passes are divided into grid size in the (x, y, and z) directions (61, 51, 21) nodes. Also, the grids size of (the glass cover and the back plate), and (upper and lower absorbent plate) are (61×3×21), and (57×3×21) nodes, respectively, as illustrated in Fig. 2.

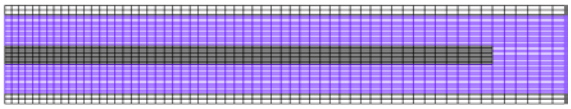

Fig. 2. Mesh of the discretized computational domain.

Hence, the energy balance equation from the six faces (south, north, east, west, top and bottom) of a control volume is given as:

$$\left(\frac{\partial^2T}{\partial x^2}\right)+\left(\frac{\partial^2T}{\partial y^2}\right)+\left(\frac{\partial^2T}{\partial z^2}\right)+S_\phi=\frac{1}{\alpha}\frac{\partial T}{\partial t} \quad \dots(2)$$

Where, S_ϕ and $\alpha=\frac{k}{\rho Cp}$ are referred to the source term and the diffusivity of solid material, respectively.

The mathematical model of paraffin wax-PCM is based on the enthalpy transforming method, represented the relationship between enthalpy and temperature in the energy equation of PCM. The viscous dissipation and convective term are negligible. The three-dimensional energy equation model was found by Cao[18]as follows:

Solid-phase region:

$$\frac{\partial}{\partial x}\left(k_s\frac{\partial T}{\partial x}\right)+\frac{\partial}{\partial y}\left(k_s\frac{\partial T}{\partial y}\right)+\frac{\partial}{\partial z}\left(k_s\frac{\partial T}{\partial z}\right)+\bar{q}=\rho\frac{\partial H}{\partial t} \quad \dots(3)$$

Liquid-phase region:

$$\frac{\partial}{\partial x}\left(k_l\frac{\partial T}{\partial x}\right)+\frac{\partial}{\partial y}\left(k_l\frac{\partial T}{\partial y}\right)+\frac{\partial}{\partial z}\left(k_l\frac{\partial T}{\partial z}\right)+\bar{q}=\rho\frac{\partial H}{\partial t} \quad \dots(4)$$

The heat capacity for each phase is identical, and the transition phase happens at a constant temperature,[19].

$$T=\begin{cases}T_{melt}+H/C_{ps} & H\le 0 \quad (solid\ phase)\\ T_{melt} & 0<H<L \quad (phase\ change)\\ T_{melt}+(H-L)/C_{pl} & H\ge L \quad (liquid\ phase)\end{cases} \dots(5)$$

And the finite-volume technique with an explicit scheme are employed to evaluate the above equations as:

$$\iiint_{\Delta V}\rho\frac{\partial H}{\partial t}=\rho\Delta V\left(\frac{H_p-H_p^\circ}{\Delta t}\right) \quad \dots(6)$$

The unsteady state model of the PCM balancing equations used the explicit scheme over a control volume,

which performed in a subroutine during the charging time is 90 min with a time step of 30 seconds to solve temperature distribution of a paraffin wax-PCM which coupled and needed within subroutine of an absorbent plate within the main program. Initially, the DP-SAH integrated with a paraffin wax-PCM system is assumed to be at an ambient temperature of $T_{am} = 25$ °C:

a) Glass cover, upper and lower absorber surfaces, and back plate:

$T_{all} = T_{am}$

b) Paraffin wax-PCM:

At $\tau = 0,\ T_{PCM} = T_{am}$

The boundary conditions for the whole system which consist of:

a) At collector cover, upper and lower absorbing surfaces, back plate, and side edges walls: (U=V=W=0), no-slip condition.

b) Boundaries surfaces of the bottom and side edges are assumed an insulated:

$$\frac{\partial \mathrm{T}}{\partial n} = 0 \ \text{, n = x, y, and z direction}$$

c) Inlet boundary conditions:

At the inlet duct of the 1st pass of the heater, the velocity and temperature profiles were assumed uniform.

$$\left.\begin{matrix} At\quad x = 0 \\ 0 < y < H_{ch1} \\ 0 < z < W \end{matrix}\right\} \quad , \quad \left.\begin{matrix} U(x,y,z) = U_{in} \\ V(x,y,z) = 0 \\ W(x,y,z) = 0 \\ T(x,y,z) = T_{in} \end{matrix}\right\} \qquad \text{... (7)}$$

For turbulence parameters:

$k_{in} = C_k u_{in}^2$

$\varepsilon_{in} = C_\mu k_{in}^{3/2}/(0.5 D_h C_\varepsilon)$ … (8)

Where C_k and C_ε are constants of ($C_k = 0.003$, $C_\varepsilon = 0.03$), [17].

d) Outlet boundary conditions

In the outlet section, a fully developed flow includes the set normal gradients to be zero, which can be written as:

$$\left.\begin{matrix} At\quad x = 0 \\ H_{ch1} + H_{pcm} < y < H_{ch2} \\ 0 < z < W \end{matrix}\right\} \quad , \frac{\partial \phi}{\partial x} = 0$$

Where; ϕ *…is referred to the independent variables of: U, V, W, T, k , and* ε

In numerical analysis, the grid size of paraffin wax-PCM is (57*12*14) nodes in the (x, y, z) directions. The computations took about 500-3500 iterations and convergence criteria is $5 * 10^{-3}$ in this study. To reach convergence with finer mesh where the difference results of an air outlet temperature is less than 2 % °C.

The useful energy rate (Q_{ua}) to the air flowing in a DPSA-collector is [20]:

$$Q_{ua} = \dot{m}_a C_{pa} (T_{out} - T_{in}) \qquad \text{… (9)}$$

Where $\dot{m}_a$, C_{pa}, and ($T_{out} - T_{in}$) were the air MFR, air heat capacity, and the air temperature rise of the collector, respectively.

In this study the bottom and edges of the, DP-SAH were insulated. Therefore, the loss of energy from the top cover of the DPSA-heater's to the ambient is considered as a major area for losses as:

$$Q_{loss} = U_{loss} A_{co} (T_{up,m} - T_{am}) \qquad \text{… (10)}$$

Where the term of U_{loss} in eq.(10) can be obtained from following equation:

$$U_{loss} = U_{top} + U_{bottom} + U_{edge} \qquad \text{… (11)}$$

Note that U_{top} , U_{bottom} , *and* U_{edge} are the overall coefficient of energy losses from the top, bottom, and edges of DPSA-heater's, respectively. Further, U_{bottom} *and* U_{edge} were neglected in this work result in the good insulation, the overall coefficient of energy loss from DPSA- heater's top is as follows can be found by Duffie and Beckman[21]:

$$U_{top} = \frac{1}{\frac{N}{\frac{C}{T_{up,m}}\left[\frac{T_{up,m} - T_{am}}{N+f}\right]^e} + \frac{1}{h_w}} + \frac{\sigma (T_{up,m} + T_{am})(T_{up,m}^2 + T_{am}^2)}{\left(\varepsilon_p + 0.0059\, N h_w\right)^{-1} + \frac{2N + f - 1 + 0.133\varepsilon_p}{\varepsilon_g} - N} \qquad \text{… (12)}$$

Where, N= number of the glass covers.

$f = \left(1 + 0.089 h_w - 0.1166 h_w \varepsilon_p\right)(1 + 0.07866 N)$

$C = 520(1 - 0.000051\beta^2)$

For $0^\circ < \beta < 70^\circ$, $\beta = collector\ tilt\ (deg)$

$e = 0.430(1 - 100/T_{up,m})$

$h_w = 2.8 + 3.3 V_w$, h_w = the wind convection coefficient.

The thermal energy storage efficiency (η_{TES}) of the solar heater states to the ratio of the retrievable energy to the storing energy of PCM [2] is as follows:

$$\eta_{TES} = \frac{Retrievable\ energy}{Retrievable\ energy + loss\ energy} = \frac{Q_{ua}}{Q_{ua} + Q_{loss}} \qquad \text{… (13)}$$

Thermal efficiency (η_{th}) of a solar heater refers to measure its performance can be represented the ratio of the useful energy gain minus the total lost energy from the collector to the intensity of solar energy during a specified period for the collector [21] as follows :

$$\eta_{th} = \frac{Q_{ua} - Q_{loss}}{I_s A_{co}} \qquad \text{… (14)}$$

Where, I_s , *and* A_{co} are represented to the solar flux intensity and the collector area, respectively.

3. RESULTS AND DISCUSSION

In order to confirm the present prediction results of the double-pass SAH performance without PCM were validated with the previous studies: the measured values found from Karim and Hawlader (2006) [12], and the mathematical values obtained by Yousef and Adam (2008) [13] of the thermal efficiency at the same operating parameters, as shown

in Fig.3. The validation of present numerical results revealed that the maximum deviation of thermal efficiency is ±16.7, and ± 3.36 % as compared to previous studies, this shows the mathematical modeling values were acceptable.

Numerical analysis was achieved to evaluate the DP-SAH performance with paraffin wax-PCM, under a constant wind speed and ambient temperature are about 1.5 m/sec 25°C, respectively. In the present results, three air mass flow rates of 0.6, 1.2, and 1.8 kg/min at a fixed solar flux of 625 W/m^2 were studied.

Figures 4 and 5 present the velocity vectors and isotherms patterns of the airflow in 1st and 2nd passes of the DP-SAH with thermal storage after 90 minute of charging period under various airflow of 0.6, 1.2, and 1.8 kg/min. The temperature distribution significantly influenced by the flow pattern in collector. The velocity vector indicates that the flow is fully developing and decreases towards the duct walls until it becomes zero at the walls, while it has a maximum value at the center of the channel, as it moves towards to the collector end and recycles airflow in the 2nd pass in opposite direction. temperature decreases with the increasing of the airflow speed indicating that this temperature difference decreases, see Fig. 5(c).

Figure 6 illustrates that temperature contours of a paraffin wax-PCM layers inside capsules during charging (melting) and discharging (freezing) periods, at fixed air mass flow rate of 0.6 kg/min and solar intensity of 625 W/m^2. During charge period for 90 minutes, the numerical results show that the paraffin layer temperature increases gradually from upper and lower absorbent surfaces as a result of the absorbed energy to melt PCM layers by heat conduction in order to store energy, see Fig 6 (a). In the discharging process, the paraffin inside capsules starts to heat the absorbent surfaces and then exchange with fluid operating at night with an optimum discharging period for 360 minutes. When PCM temperature drops slowly after melting temperature of PCM to value less than 38°C the PCM has completely solidified, as shown in Fig.6 (b).

Figure 7 displays the temperature curves of the upper and lower absorbent surfaces, paraffin wax-PCM, and outlet air in a two-pass heater with latent storing energy, for various airflow speed of 0.6, 1.2, and 1.8 kg/min during the melting/solidification processes. The results show that all temperature profiles begin to increase over time during the charging period is implemented for 90 minutes, and the upper and lower absorbent plates are the hottest part of the heater. From the upper and lower of storage indicating the paraffin wax-PCM begins to melt. The absorbed energy is storing as sensible energy and raised the temperature of a paraffin wax which reaches 38 °C, and so the fusion starts. As soon as the melting point of PCM reaches 43°C and saves stable, signifying that the total PCM in the rectangular capsule has fully melted. It was also detected that maximum temperature difference reach at the peak level during the low range of the airflow speed.

By increasing air MFR, the results showed that low absorbed energy received by the absorbent surfaces during a prolonging period of the charging process about of 90 min lead to minimum temperature attained by paraffin wax during this process as compared to other air MFR and partially PCM is melting, as seen in Fig. 7(b and c). After the melting period the discharge period starts, the temperature profiles continue to drop slowly versus the discharge period. When PCM temperature drops to 38°C the PCM has completely solidified. After an hour of the initial freezing time, the temperatures of the upper and lower absorbent surfaces and the PCM melting point are nearly identical, this can be attributed to energy storage in PCM and at night the heat is transferred to the absorbent surface by conduction. Moreover, their results observed that the optimal freezing period and the air temperature rise of the heater were reached about 210 minutes with (12 – 1.5 °C), 150 minutes with (7.5 – 1.4°C), and 120 minutes with (5.5 – 1.5 °C), at airflow speed of 0.6, 1.2, and 1.8 kg/min, respectively for solar energy of 625 W/m^2. Thus, it is inferred that the solar collector with storing energy can be used even at night.

Figures (8-11) show the influence of airflow speed on the temperatures of the absorbent surfaces and paraffin wax melting point, and air versus melting/freezing period for different mass flow rates; 0.6, 1.2, and 1.8 kg/min at same averaged solar intensity of 625 W/m^2, respectively. The results show that the increased airflow rate leads to delayed melting time and also lower the melting temperature of PCM during the charging process. As well as, the freezing time is dependent on the air MFR by inverse relation. This can be attributed to a decrease in the exchanging heat of the absorbent surfaces with air flowing when an increase in airflow flow rate, as revealed in Fig.8. Also, it can be observed that the results of the PCM melting point and the exit air temperature curves decrease correspondingly as the air MFR increases from 0.6 to 1.8 kg/min in the air heater, as seen Figures 9 and 10. The maximum values attained by paraffin wax-PCM melting point and air temperature rise in the DP-SAH with PCM during this process were approximately of 44.55°C and 12°C (see Fig. 11), respectively.

The effect of airflow speed on the useful energy rate during charge and discharge time at fixed solar radiation, as described in Fig. 12. Obviously, it can be noticed that the increased useful power when the value of air MFR was increased. Finally, the thermal storage efficiency of the DP-SAH with PCM versus melting/freezing period at various air MFR of 0.6, 1.2, and 1.8 kg/min, as displayed in Fig.13. It is clear that higher thermal storing efficiency through absorbed solar energy within PCM layers by heat conduction during the charging or (melting) process. In the discharging or (freezing) process, the storage performance increased as airflow speed increases. At the low airflow speed led to the prolonging time of storage energy compared with another air MFR due to higher storing energy.

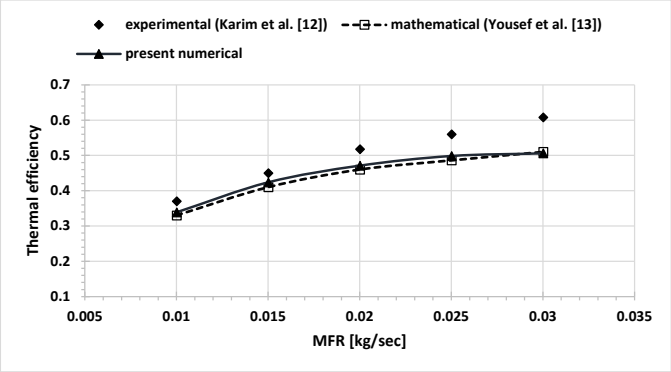

Fig. 3. Comparison of the thermal performance of present numerical study with previous studies.

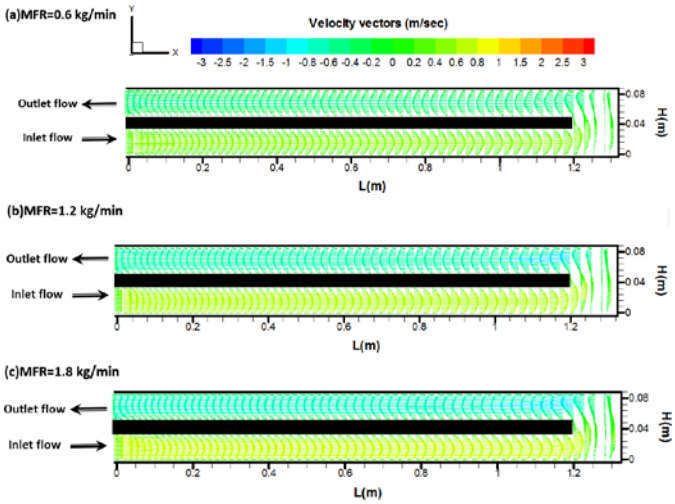

Fig. 4. Velocity vectors of airflow along the DP-SAH with PCM at constant solar energy of 625 W/m^2 for different air MFR: (a) MFR= 0.6 kg/min, (b) MFR= 1.2 kg/min, and (c) MFR= 1.8 kg/min.

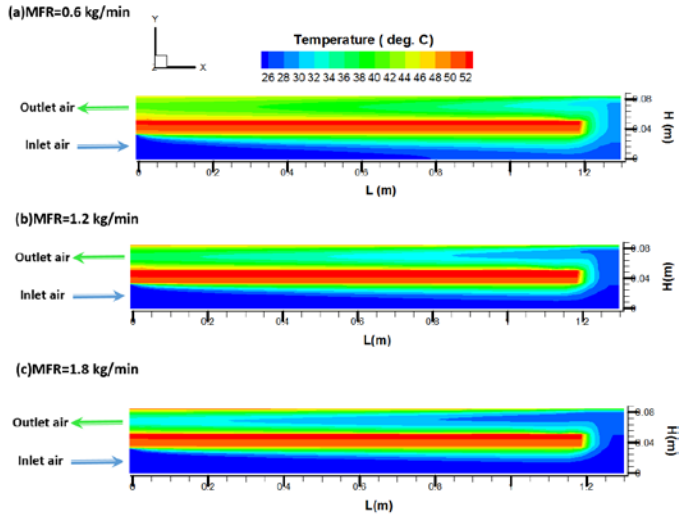

Fig. 5. Isotherms of airflow along the DP-SAH with PCM at constant solar energy of 625 W/m^2 for different air MFR: (a) MFR= 0.6 kg/min, (b) MFR= 1.2 kg/min, and (c) MFR= 1.8 kg/min.

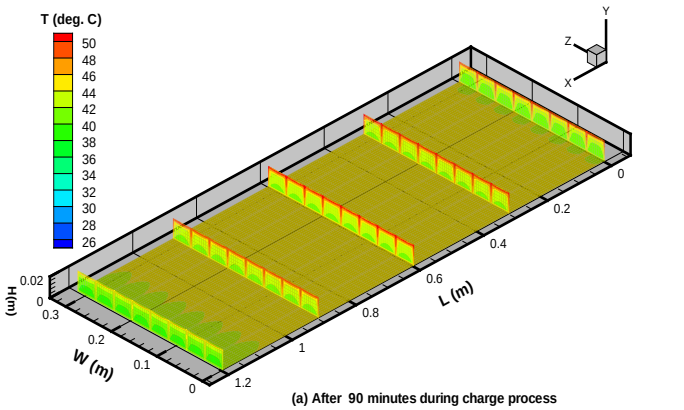

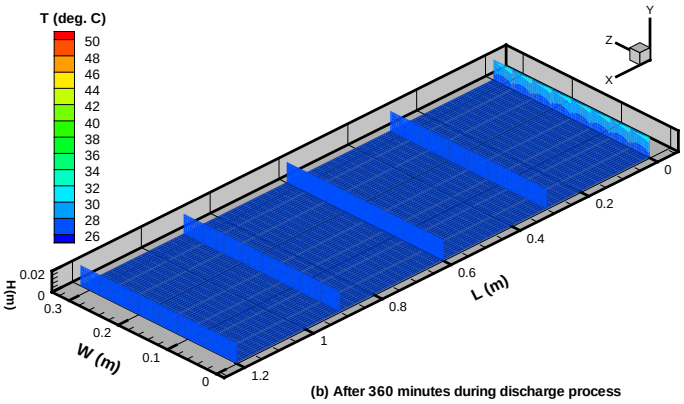

Fig. 6. Isotherms for the rectangular multiple capsules filled with PCM for fixed air mass flow rate of 0.6 kg/min: (a) during charging period under average solar flux of 625 W/m^2, and (b) (a) during discharging period when average solar flux equal to zero (at night).

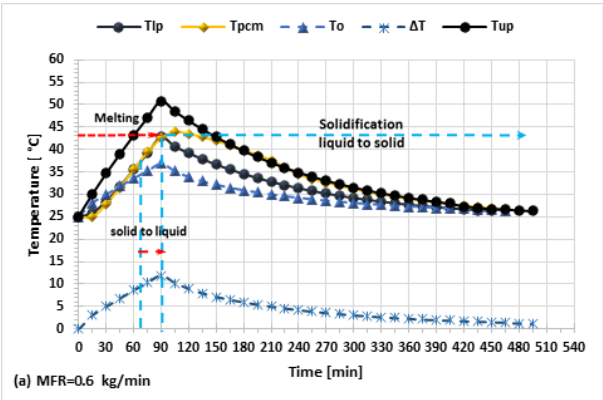

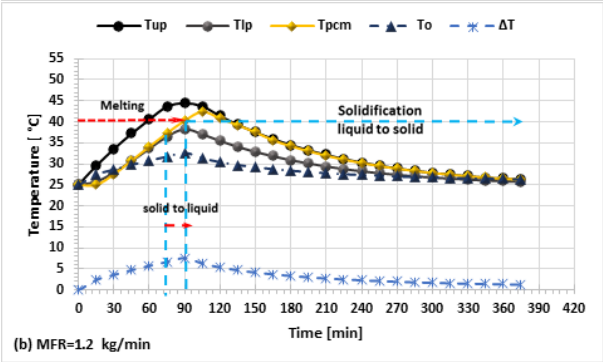

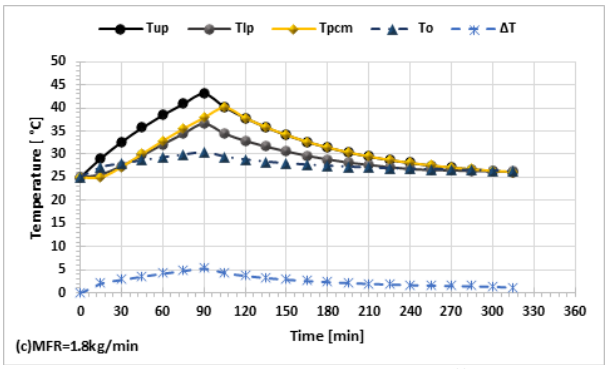

Fig.7 The average air, absorbent plate and wax paraffin temperature variations in the DP-SAH with PCM versus charge and discharge time for I_s = 625 W/m^2 at various air mass flow rates: (a) 0.6 kg/min, (b) 1.2 kg/min, and (c) 1.8 kg/min.

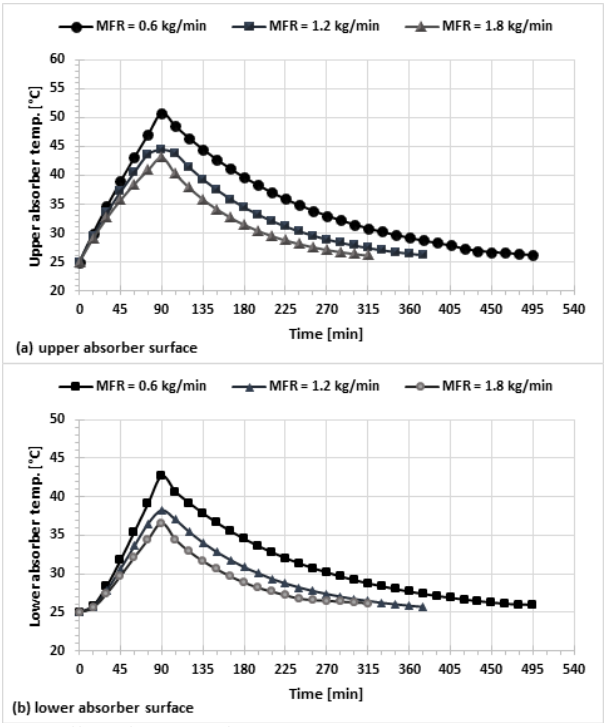

Fig.8 Effect of air mass flow rate on an absorber plate temperature: (a) upper surface, and (b) lower surface, during charge and discharge time at solar irradiation of 625 W/m^2.

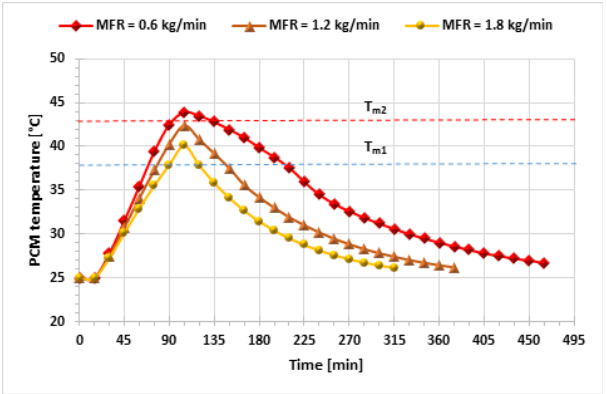

Fig.9 Effect of air mass flow rate on wax paraffin-PCM temperature rise during charge and discharge time at solar irradiation of 625

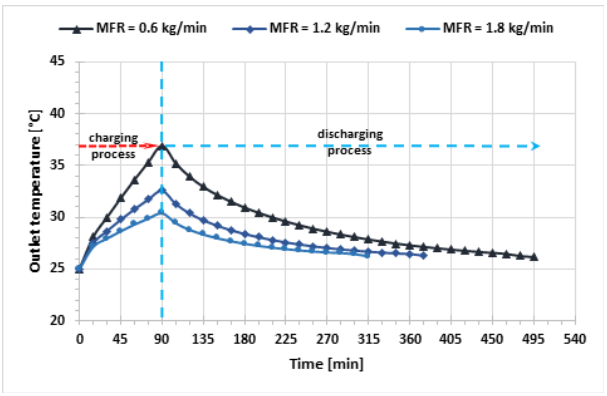

Fig.10 Effect of air mass flow rate on outlet air temperature during charge and discharge time at solar irradiation of 625 W/m^2.

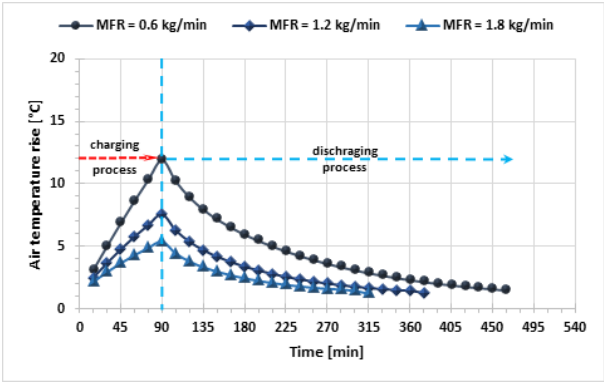

Fig.11 Effect of air mass flow rate on air temperature rise during charge and discharge time at solar irradiation of 625 W/m^2.

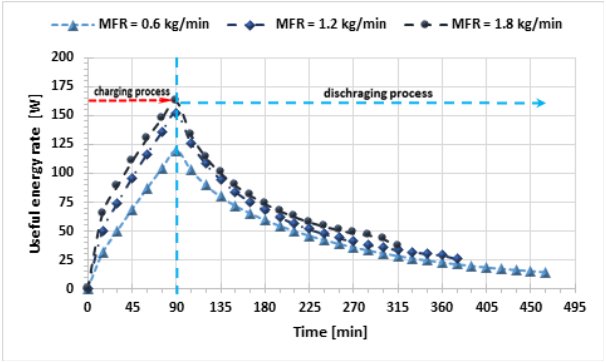

Fig.12 Effect of air mass flow rate on a paraffin wax-PCM temperature during charge and discharge time at solar irradiation of

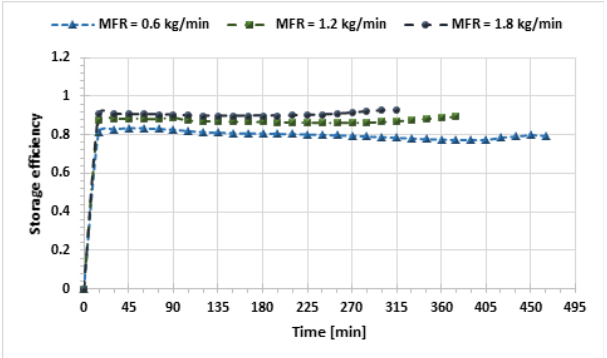

Fig.13 Effect of air mass flow rate on a paraffin wax-PCM temperature during charge and discharge time at solar irradiation of

4. CONCLUSION

In the present computational analysis, the main conclusions can be summarized as follows:

1- The maximum values of air temperatures rise obtained across the two-pass solar air heater with PCM was approximately of 12 °C , at an airflow speed of 0.6 kg/min and irradiance of 625 W/m^2.
2- The results show that the delaying melting time and also lower the melting temperature of PCM by increasing airflow speed during the charging process. As well as, the freezing period is dependent on the airflow speed by inverse relation.
3- The data results represent that the useful energy rate and thermal storage efficiency were a strong dependence on the airflow speed.
4- Finally, it can be detected that the optimal freezing period and the air temperature rise of the collector were reached of 210 minutes with (12 – 1.5 °C), 150 minutes with (7.5 – 1.4°C), and 120 minutes with (5.5 – 1.5 °C), at airflow speed of 0.6, 1.2, and 1.8 kg/min, respectively for solar energy of 625 W/m^2.

REFERENCES:

[1] K.-D. Jäger, O. Isabella, A. H. Smets, R. A. van Swaaij, and M. Zeman, *Solar Energy: Fundamentals, Technology and Systems*: UIT Cambridge, 2016.

[2] M. M. Alkilani, K. Sopian, and S. Mat, "Fabrication and experimental investigation of PCM capsules integrated in solar air heater," *American Journal of Environmental Sciences*, vol. 7, p. 542, 2011.

[3] H. F. Oztop, F. Bayrak, and A. Hepbasli, "Energetic and exergetic aspects of solar air heating (solar collector) systems," *Renewable and Sustainable Energy Reviews*, vol. 21, pp. 59-83, 2013.

[4] S. M. Shalaby, M. A. Bek, and A. A. El-Sebaii, "Solar dryers with PCM as energy storage medium: A review," *Renewable and Sustainable Energy Reviews*, vol. 33, pp. 110-116, 2014.

[5] K. A. Joudi and A. A. Farhan, "Greenhouse heating by solar air heaters on the roof," *Renewable Energy*, vol. 72, pp. 406-414, 2014.

[6] V. Smil, *General energetics: energy in the biosphere and civilization* vol. 369: Wiley New York, 1991.

[7] M. Alkilani, K. Sopian, S. Mat, and M. Alghoul, "Output air temperature prediction in a solar air heater integrated with phase change material," *European Journal of Scientific Research*, vol. 27, pp. 334-341, 2009.

[8] H. E. Fath, "Thermal performance of a simple design solar air heater with built-in thermal energy storage system," *Renewable energy*, vol. 6, pp. 1033-1039, 1995.

[9] S. Shalaby, M. Bek, and A. El-Sebaii, "Solar dryers with PCM as energy storage medium: A review," *Renewable and Sustainable Energy Reviews*, vol. 33, pp. 110-116, 2014.

[10] A. Acır and M. E. Canlı, "Investigation of fin application effects on melting time in a latent thermal energy storage system with phase change material (PCM)," *Applied Thermal Engineering*, vol. 144, pp. 1071-1080, 2018.

[11] P. Charvat, M. Ostry, T. Mauder, and L. Klimes, "A solar air collector with integrated latent heat thermal storage," in *EPJ Web of Conferences*, 2012, p. 01028.

[12] M. A. Karim and M. Hawlader, "Performance investigation of flat plate, v-corrugated and finned air collectors," *Energy*, vol. 31, pp. 452-470, 2006.

[13] B. Yousef and N. Adam, "Performance analysis for flat plate collector with and without porous media," *Journal of Energy in Southern Africa*, vol. 19, pp. 32-42, 2008.

[14] S. ASHRAE, "93-77 1977 Methods of testing to determine the thermal performance of solar collectors, American Society of Heating," *Refrigeration and Air Conditioning Engineers, New York*.

[15] T. Josyula, S. Singh, and P. Dhiman, "Numerical investigation of a solar air heater comprising longitudinally finned absorber plate and thermal energy storage system," *Journal of Renewable and Sustainable Energy*, vol. 10, p. 055901, 2018.

[16] H. K. Versteeg and W. Malalasekera, *An introduction to computational fluid dynamics: the finite volume method*: Pearson Education, 2007.

[17] B. E. Launder and D. B. Spalding, "The numerical computation of turbulent flows," in *Numerical Prediction of Flow, Heat Transfer, Turbulence and Combustion*, ed: Elsevier, 1983, pp. 96-116.

[18] Y. Cao, A. Faghri, and W. S. Chang, "A numerical analysis of Stefan problems for generalized multi-dimensional phase-change structures using the enthalpy transforming model," *International journal of heat and mass transfer*, vol. 32, pp. 1289-1298, 1989.

[19] T. Norton, A. Delgado, E. Hogan, P. Grace, and D.-W. Sun, "Simulation of high pressure freezing processes by enthalpy method," *Journal of food engineering*, vol. 91, pp. 260-268, 2009.

[20] J. M. Hassan, Q. J. Abdul-Ghafour, and A. A. Mohammed, "Experimental performance of a double pass solar air heater with thermal storage," *Advances in Natural and Applied Sciences*, vol. 10, pp. 84-94, 2016.

[21] J. A. Duffie and W. A. Beckman, *Solar engineering of thermal processes*: John Wiley & Sons, 2013.

Nomenclature

A	*area (m^2)*
Cp	*heat capacity (J/kg.K)*
D_h	*hydraulic diameter (m)*
W	*collector width (m)*
H_{ch1}	*the height of 1st channel (m)*
H_{ch2}	*the height of 2nd channel (m)*
H_{PCM}	*the height of paraffin wax-PCM (m)*
h	*heat transfer coefficient ($W/m^2.°C$)*
H	*enthalpy (kJ/kg)*
L	*latent heat (kJ/kg)*
$\bar{q}$	*average heat generation(W/m^3)*
k	*Thermal conductivity (W/m.K)*
T	*temperature (°C)*
a,b	*the coefficient in the discretization equation*
I_s	*solar intensity (W/m^2)*
V	*velocity of airflow (m/sec)*
Q_{ua}	*useful energy rate of air (W)*
Q_{loss}	*lost energy rate to the ambient (W)*
$\dot{m}_a$	*air mass flow rate (kg/min)*

Greek letters

ρ	*density (kg/m^3)*
α	*absorptivity*
ε	*emissivity*
ϕ	*any of the variables to be solved*
Δt	*time difference (sec)*
η_{TES}	*thermal energy storage efficiency*
η_{th}	*thermal efficiency*

Subscripts

f1	*airflow in 1st pass*
f2	*airflow in 2nd pass*
a	*air*
am	*ambient*
w	*wind*
g	*glass cover*
up	*upper absorbent plate*
lp	*lower absorbent plate*
bp	*backplate*
l	*liquid*
s	*solid*
co	*collector*
o	*outlet*
i	*inlet*
m	*mean*
	melting point